REF: A0724.0713

INFLUENCE OF FRICTION ON GEAR DYNAMICS

Paulo Fernandes[1*], José Dias Rodrigues[2], Jorge Seabra[2], and Joaquim Sabino[1]
[1]Instituto Superior de Engenharia, Instituto Politécnico do Porto, Portugal
[2]Faculdade de Engenharia, Universidade do Porto, Portugal
Email: [(*)]pbf@isep.ipp.pt

SYNOPSIS

Sliding friction between meshing teeth can be a very important of noise and vibration excitation source in geared systems. This study presents a single degree of freedom torsional model for a FZG type C single gear pair. Starting from a base dynamic model with time varying mesh stiffness as the only internal excitation, the influence of additional effects is gradually considered, namely, constant friction coefficients and time varying output torques. In particular, sliding friction is modeled as external and internal linear time varying excitation. On the other hand, time varying output torques are also considered as alternative of constant driven torque.

The gear's rotational vibrations are calculated by Runge-Kutta method for different combinations of rational speeds, input torques and friction coefficients. The results indicate that dynamic transmission errors calculated from modeling the friction force as external and internal excitation are quite different, especially when contact point moves ahead of pitch point. However the influence of time variations on output torque is very reduced.

1. INTRODUCTION

Gears can be found in a wide variety of transmission systems including automotive, aerospace, industrial applications, etc. Even though they exhibit considerable technical advantages like high power to weight ratio and efficiency, normal operating conditions can be seriously affected by a variety of external and internal excitation.

Dynamic analysis of geared systems is a major consideration in gear design, and essential for understanding, controlling and eliminating noise and vibration problems. Excessive dynamic loads caused by different sources like inadequate lubrication, manufacturing and/or installation problems, inappropriate operating conditions and design insufficiencies can originate considerable gear noise and vibration inconvenients. Especially when static loads are amplified during gear meshing action generating high gear dynamic meshing loads.

Besides prior interest of many researchers, the first studies in gear dynamics started in the 20's decade (Parey, 2003), mainly to predict the tooth dynamic load for high speed gears. Since then, numerous dynamic models have been published in literature concerned with gear noise and vibration. A complete and extended review of the mathematical models used in gear dynamics was given by Özguven, 1988. The authors classified the mathematical models in five groups: Simple Dynamic Factor Models, Models with Tooth Compliance, Models for Gear Dynamics, Models for Geared Rotor Dynamics and Models for Torsional Vibrations. In general, the proposed models in the literature differ from each other according to the following included effects and solution methods: degrees of freedom (one, multi, infinite), gear types (spur, helical, bevel, worn), mechanical elements (shafts, bearings, gear housing, etc.), solution techniques (direct numerical integration, harmonic balance method, Floquet

theory), type of response (steady state or transient), excitation (low or high frequency) and other very important effects such as can also be included like gear and mounting errors, friction, tooth modifications and wear. However, and besides this huge number of possibilities it is assumed that transmission error and variation in mesh stiffness are two fundamental primary sources of gear excitation.

The literature on gear teeth rolling/sliding friction is sparse, although it is believed to be one of the primary excitation for noise and vibration in geared power transmissions (Gunda, 2003). Due to the sense reversion at pitch point, friction can be associated with a large oscillatory component especially at high torques and low speeds due to high forces in the sliding direction (Vaishya, 2003), even though sliding force amplitudes are small when compared to the mean transmitted loads. The sliding friction effects can be modeled as an external or internal excitation. As external, sliding friction has the same fundamental period of the gear mesh cycle and respective terms are placed in the right-hand side of the equation of motion. As internal, sliding friction can be based on the dynamic mesh force resulting in a linear dynamic model which also affects the homogenous part of the equation of motion, or resulting in a non-linear dynamic model where friction is clearly dependent of the instantaneous sliding velocity. Vaishya, 2001 compared dynamic transmission error of external and internal friction formulations (linear and non linear time varying systems) and concluded that for non-resonant conditions both yield identical results, except in the neighborhood of the pitch point zone. Kuang, 2001 proposed a dynamic model with time varying friction coefficient along the meshing line which in turn depends of sliding velocity and instantaneous viscosity of the lubricant film. Finally, Howard, 2001 considers the importance of friction to simulate the motion perpendicular to the meshing line, coupling as consequence the torsional and transverse motions of the gears and shafts.

The aim of this paper is to study the influence of friction effects on the dynamic behavior of a FZG type C gear. A single degree of freedom torsional model of gear pair is proposed considering firstly the effects of time-varying mesh stiffness and viscous damping, and subsequently, the effects of constant friction coefficient and time varying output torques. The solutions of the differential equation of motion are obtained through the Runge-Kutta method.

2. DYNAMIC MODEL FOR A SPUR GEAR PAIR

A spur gear pair is shown in Figure 1, in which T_p and T_w represent the input and output torque, respectively (subscripts p and w stand for the pinion and the wheel respectively). R_p and R_w are the radii of the base circles, J_p and J_w are the polar moments of inertia while c is the total mesh damping. As time-varying parameters θ_p and θ_w denote the vibratory angular displacement from the mean position, k the total mesh stiffness and ε is the unloaded static transmission error. Note that k and ε are here assumed to be explicit functions of time.

Considering a linear time-varying system with pinion torque as positive, the equations of torsional motion can be written as follows :

$$\begin{cases} J_p \ddot{\theta}_p = T_p - k(R_p\theta_p - R_w\theta_w - \varepsilon)R_p - c(R_p\dot{\theta}_p - R_w\dot{\theta}_w - \dot{\varepsilon})R_p \\ J_w \ddot{\theta}_w = -T_w + k(R_p\theta_p - R_w\theta_w - \varepsilon)R_w + c(R_p\dot{\theta}_p - R_w\dot{\theta}_w - \dot{\varepsilon})R_w \end{cases} \quad (1)$$

Both equations constitute a semi-definite system with two degrees of freedom θ_p and θ_w that can be reduced to a single degree of freedom introducing the dynamic transmission error x (DTE) as:

$$x = R_p\theta_p - R_w\theta_w \tag{2}$$

$$m_e \ddot{x} + c(\dot{x} - \dot{\varepsilon}) + k(x - \varepsilon) = \frac{J_w R_p T_p + J_p R_w T_w}{J_p R_w^2 + J_w R_p^2} = \frac{T_p}{R_p} = \frac{T_w}{R_w} = F_0 \tag{3}$$

$$m_e = \frac{J_w * J_p}{J_p R_w^2 + J_w R_p^2} \tag{4}$$

Here m_e is the equivalent mass of spur gear pair and F_0 the static transmitted load.

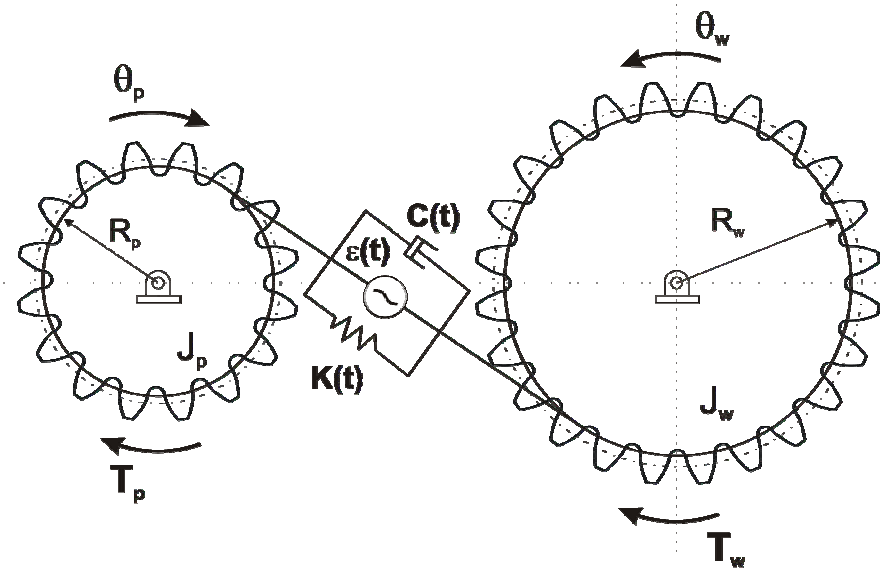

Figure 1. Dynamic model of a spur gear pair.

By definition the friction force is the resistance to motion whenever solid A slides over B, and can be expressed as follows

$$\overrightarrow{F_a}^{A/B} = -\mu \cdot \left\| \overrightarrow{F_n} \right\| \cdot \frac{\overrightarrow{v_{A/B}}}{\left\| \overrightarrow{v_{A/B}} \right\|} \tag{5}$$

where μ is the friction coefficient, F_n the normal force and $v_{A/B}$ the sliding velocity.

Considering now the meshing between pinion and wheel teeth, the friction force may result time varying due to variations of sliding velocity term, normal force and/or friction coefficient. Even if normal force and friction coefficient are assumed constant along the gear meshing line, at least the unitary vector $\frac{\overrightarrow{v_{A/B}}}{\left\| \overrightarrow{v_{A/B}} \right\|}$ changes its sign at pitch point (+1 to -1, or -1 to +1), being null at pitch point. The analytical analysis of sliding velocities along the meshing line is treated on Appendice A.

Figure 2 shows friction force analysis between pinion and wheel teeth as the contact point(s) moves along the meshing line. Normal forces and friction forces acting on pinion and wheel

teeth are represented above and bellow of meshing line respectively. Three different situations must be highlighted. First, when contact points are at double contact zone, second, when single contact point is on right of pitch point and third, when single contact point is on left of pitch point. At double contact zone, the normal force is divided by first and second contact points. Moreover friction forces acting at first and second contact on pinion (or wheel) are at opposite senses. At single contact zones, on left and right of pitch point, the normal force is exclusively supported by one teeth pair and friction forces are also at opposite directions, regarding pitch point.

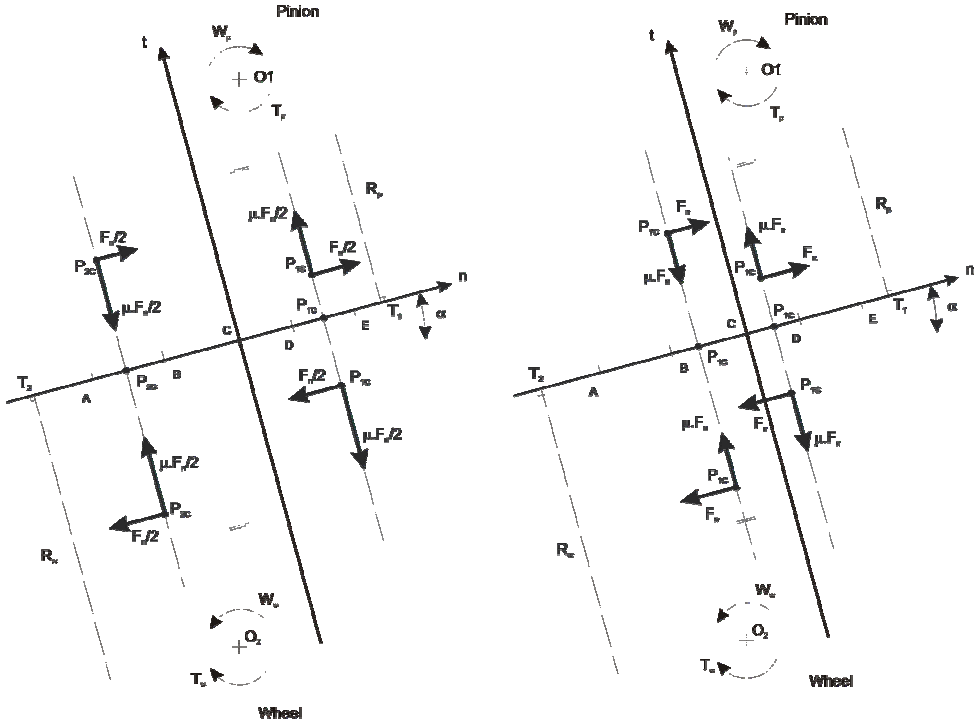

Figure 2. Free body diagram of normal and friction forces acting along meshing line.

Regarding the equations of torsional motion (1) of a spur gear pair, this study considers two different friction force's alternatives. In the first alternative, the friction force is considered as external excluding all dynamic effects of normal force, and so,

$$F_n = F_0 = \frac{T_p}{R_p} = \frac{T_w}{R_w} \tag{6}$$

In the second alternative, the friction force has an internal action and normal force is now dependent of dynamic transmission error (DTE) as follows

$$F_n = c(\dot{x} - \dot{\varepsilon}) + k(x - \varepsilon) \tag{7}$$

2.1 External action of friction force with constant friction coefficient

This first alternative to the base model considers the action of friction force exclusively as an external force, and independent of dynamic response of spur gear. Although considered as an external action, and as seen before for this type of model, friction force may be time varying

along meshing line. On the other side, contact points and respective moment arms also change over the time, forcing friction torques acting on pinion and wheel as being time varying to.

The three important time instants of a mesh cycle, *ta*, *tb* and *tc*, are defined as finish of double contact zone, instant of pitch point and finish of mesh cycle, respectively.

A new set of dynamic equations for torsional motion of spur gear pair for each zone (double contact and two single contact zones around pitch point), and correspondent final dynamic equations with 1 degree of freedom can be written as follows:

- **Double tooth contact zone, $0 \le t < t_a$.**

First tooth contact point P1C lies along ED zone, and second tooth contact point P2C along BA zone (see Figure 2):

$$\begin{cases} J_p \ddot{\theta}_p = T_p - k(R_p\theta_p - R_w\theta_w - \varepsilon)R_p - c(R_p\dot{\theta}_p - R_w\dot{\theta}_w - \dot{\varepsilon})R_p + \dfrac{\mu}{2}\cdot F_0 \cdot \left(\overbrace{\overline{T_1P_{1C}}(t) - \overline{T_1P_{2C}}(t)}^{=-p_b} \right) \\ J_w \ddot{\theta}_w = -T_w + k(R_p\theta_p - R_w\theta_w - \varepsilon)R_w + c(R_p\dot{\theta}_p - R_w\dot{\theta}_w - \dot{\varepsilon})R_w - \dfrac{\mu}{2}\cdot F_0 \cdot \left(\overbrace{\overline{T_2P_{1C}}(t) - \overline{T_2P_{2C}}(t)}^{=p_b} \right) \end{cases} \tag{8}$$

$$m_e \ddot{x} + c(\dot{x} - \dot{\varepsilon}) + k(x - \varepsilon) = \frac{J_w R_p T_p + J_p R_w T_w}{J_p R_w^2 + J_w R_p^2} + F_0 \cdot \frac{\mu}{2} \cdot \left[\frac{-J_w R_p p_b + J_p R_w p_b}{J_p R_w^2 + J_w R_p^2} \right] \tag{9}$$

with moment arms determined by,

$$\begin{aligned} \left[\overline{T_1P_{1C}}(t)\right] &= \overline{T_1E} + w_p \cdot R_p \cdot t \\ \left[\overline{T_1P_{2C}}(t)\right] &= \overline{T_1T_2} - \overline{T_1P_{1C}}(t) = \overline{T_1T_2} - \overline{T_1E} - w_p \cdot R_p \cdot t \\ \left[\overline{T_2P_{1C}}(t)\right] &= \overline{T_1P_{1C}}(t) + \overline{EB} = \overline{T_1E} + w_p \cdot R_p \cdot t + \overline{EB} \\ \left[\overline{T_2P_{2C}}(t)\right] &= \overline{T_1T_2} - \overline{T_1P_{2C}}(t) = \overline{T_1T_2} - \overline{T_1E} - w_p \cdot R_p \cdot t \end{aligned} \tag{10}$$

In above equations the term $\frac{\mu}{2}$ express an equal load sharing amongst the teeth and p_b represents the base pitch.

- **Single tooth contact zone at right of pitch point, $t_a \le t < t_b$.**

Tooth contact point P1C lies along DC zone (see Figure 2):

$$\begin{cases} J_p \ddot{\theta}_p = T_p - (R_p\theta_p - R_w\theta_w - \varepsilon)R_p - c(R_p\dot{\theta}_p - R_w\dot{\theta}_w - \dot{\varepsilon})R_p + \mu \cdot F_0 \cdot \overline{T_1P_{1C}}(t) \\ J_w \ddot{\theta}_w = -T_w + k(R_p\theta_p - R_w\theta_w - \varepsilon)R_w + c(R_p\dot{\theta}_p - R_w\dot{\theta}_w - \dot{\varepsilon})R_w - \mu \cdot F_0 \cdot \overline{T_2P_{1C}}(t) \end{cases} \tag{11}$$

$$m_e \ddot{x} + c(\dot{x} - \dot{\varepsilon}) + k(x - \varepsilon) = \frac{J_w R_p T_p + J_p R_w T_w}{J_p R_w^2 + J_w R_p^2} + F_0 \cdot \mu \cdot \left[\frac{J_w R_p \overline{T_1P_{1C}}(t) + J_p R_w \overline{T_2P_{1C}}(t)}{J_p R_w^2 + J_w R_p^2} \right] \tag{12}$$

- **Single tooth contact zone a left ofpitch point, $t_b \leq t < t_c$.**

Tooth contact point P1C lies along CB zone (see Figure 2):

$$\begin{cases} J_p \ddot{\theta}_p = T_p - k(R_p\theta_p - R_w\theta_w - \varepsilon)R_p - c(R_p \dot{\theta}_p - R_w \dot{\theta}_w - \dot{\varepsilon})R_p - \mu \cdot F_0 \cdot \overline{T_1P_{1C}}(t) \\ J_w \ddot{\theta}_w = -T_w + k(R_p\theta_p - R_w\theta_w - \varepsilon)R_w + c(R_p \dot{\theta}_p - R_w \dot{\theta}_w - \dot{\varepsilon})R_w + \mu \cdot F_0 \cdot \overline{T_2P_{1C}}(t) \end{cases} \quad (13)$$

$$m_e \ddot{x} + c(\dot{x} - \dot{\varepsilon}) + k(x - \varepsilon) = \frac{J_w R_p T_p + J_p R_w T_w}{J_p R_w^2 + J_w R_p^2} + F_0 \cdot \mu \cdot \left[\frac{-J_w R_p \overline{T_2P_{1C}}(t) - J_p R_w \overline{T_1P_{1C}}(t)}{J_p R_w^2 + J_w R_p^2} \right] \quad (14)$$

Looking and comparing the last terms of equations (8), (11) and (13) it is interesting to note that pinion and wheel friction torques can be positive or negative. A negative pinion friction torque opposes to the pinion's movement, while a positive wheel friction torque has a similar effect for wheel's movement and *vice versa*. Additionally, equations (9), (12) and (14) are very similar to equation (3) except the 3 terms added and related with friction. As these 3 terms together represent a piecewise periodic function, a Fourier series representation can solve this discontinuity problem (Velex, 2002).

2.2 Internal action of friction the force with constant friction coefficient

An alternative formulation to external action of the friction force is to consider an internal action, where the friction force along meshing line depends now from normal dynamic force, instead of static force. As a consequence, the dynamic terms of friction torques of the governing equations pass from second to first members. Systems and respective final equations for 3 individual contact zones are given by,

- **Double tooth contact zone, $0 \leq t < t_a$.**

First tooth contact point P1C lies along ED zone, and second tooth contact point P2C along BA zone (see Figure 2):

$$\begin{cases} J_p \ddot{\theta}_p = T_p - k(R_p\theta_p - R_w\theta_w - \varepsilon)R_p - c(R_p \dot{\theta}_p - R_w \dot{\theta}_w - \dot{\varepsilon})R_p + \frac{\mu}{2} \cdot F_n \cdot \left(\overline{T_1P_{1C}}(t) - \overline{T_1P_{2C}}(t) \right) \\ J_w \ddot{\theta}_w = -T_w + k(R_p\theta_p - R_w\theta_w - \varepsilon)R_w + c(R_p \dot{\theta}_p - R_w \dot{\theta}_w - \dot{\varepsilon})R_w - \frac{\mu}{2} \cdot F_n \cdot \left(\overline{T_2P_{1C}}(t) - \overline{T_2P_{2C}}(t) \right) \end{cases} \quad (15)$$

$$\begin{aligned} m_e \ddot{x} + \left(c(\dot{x} - \dot{\varepsilon}) + k(x - \varepsilon) \right) \cdot \left[1 - \frac{\mu}{2} \cdot \left[\frac{-J_w R_p p_b + J_p R_w p_b}{J_p R_w^2 + J_w R_p^2} \right] \right] = \\ \frac{J_w R_p T_p + J_p R_w T_w}{J_p R_w^2 + J_w R_p^2} = \frac{T_p}{R_p} = \frac{T_w}{R_w} = F_0 \end{aligned} \quad (16)$$

The term $\frac{\mu}{2}$ reveals that two pairs of teeth share equal dynamic loads.

- **Single tooth contact zone at right of pitch point, $t_a \le t < t_b$.**

Tooth contact point P1C lies along DC zone (see Figure 2):

$$\begin{cases} J_p \ddot{\theta}_p = T_p - k(R_p\theta_p - R_w\theta_w - \varepsilon)R_p - c(R_p\dot{\theta}_p - R_w\dot{\theta}_w - \dot{\varepsilon})R_p + \mu \cdot F_n \cdot \overline{T_1P_{1C}}(t) \\ J_w \ddot{\theta}_w = -T_w + k(R_p\theta_p - R_w\theta_w - \varepsilon)R_w + c(R_p\dot{\theta}_p - R_w\dot{\theta}_w - \dot{\varepsilon})R_w - \mu \cdot F_n \cdot \overline{T_2P_{1C}}(t) \end{cases} \tag{17}$$

$$\begin{aligned} m_e \ddot{x} + \left(c(\dot{x} - \dot{\varepsilon}) + k(x - \varepsilon)\right) \cdot \left[1 - \mu \cdot \left[\frac{J_w R_p \overline{T_1P_{1C}}(t) + J_p R_w \overline{T_2P_{1C}}(t)}{J_p R_w^2 + J_w R_p^2}\right]\right] = \\ = \frac{J_w R_p T_p + J_p R_w T_w}{J_p R_w^2 + J_w R_p^2} = \frac{T_p}{R_p} = \frac{T_w}{R_w} = F_0 \end{aligned} \tag{18}$$

- **Single tooth contact zone at left of pitch point, $t_b \le t < t_c$.**

Tooth contact point P1C lies along CB zone (see Figure 2):

$$\begin{cases} J_p \ddot{\theta}_p = T_p - k(R_p\theta_p - R_w\theta_w - \varepsilon)R_p - c((R_p\dot{\theta}_p - R_w\dot{\theta}_w - \dot{\varepsilon}))R_p - \mu \cdot F_n \cdot \overline{T_1P_{1C}}(t) \\ J_w \ddot{\theta}_w = -T_w + k(R_p\theta_p - R_w\theta_w - \varepsilon)R_w + c((R_p\dot{\theta}_p - R_w\dot{\theta}_w - \dot{\varepsilon}))R_w + \mu \cdot F_n \cdot \overline{T_2P_{1C}}(t) \end{cases} \tag{19}$$

$$\begin{aligned} m_e \ddot{x} + \left(c(\dot{x} - \dot{\varepsilon}) + k(x - \varepsilon)\right) \cdot \left[1 - \mu \cdot \left[\frac{-J_w R_p \overline{T_2P_{1C}}(t) - J_p R_w \overline{T_1P_{1C}}(t)}{J_p R_w^2 + J_w R_p^2}\right]\right] = \frac{J_w R_p T_p + J_p R_w T_w}{J_p R_w^2 + J_w R_p^2} = \\ = \frac{T_p}{R_p} = \frac{T_w}{R_w} = F_0 \end{aligned} \tag{20}$$

Like as in the case of the external formulation, it is also possible to represent the 3 friction torque dynamic expressions through Fourier series. This allows a complete definition of an unique dynamic equation for torsional motion with three conditions, each one depending of time and position of contact point(s) along the meshing line.

2.3 Alternative output torque for the dynamic model with external action of the friction force

Both formulations employed in this study consider constant output torque which is equal to input torque times the gear ratio, i.e., $T_w = i * T_p$. However the presence of friction phenomenon may contradict this assumption, especially when the friction coefficient is considerably higher increasing gear power losses and decreasing gear efficiency. To examine the influence of friction on the output torque, three new alternative expressions (time varying) of wheel torque are derived. In the following proposed expressions an assumption is

considered regarding the angular acceleration of the pinion and whell, $\ddot{\theta}_p$ and $\ddot{\theta}_w$. Cancelling both accelerations of equations (8), (11) and (13) and equalizing respective dynamic mesh forces, after some algebraic manipulations, the output torque functions $T_w(t)$ and respective wheel efficiency $\eta(t)$ for each contact zone can be written in the following form:

- **Double tooth contact zone, $0 \le t < t_a$.**

First tooth contact point P1C lies along ED zone, and second tooth contact point P2C along BA zone (see Figure 2):

$$T_w(t) = \left[T_p - \frac{\mu}{2} \cdot F_0 \cdot p_b \right] \cdot \frac{R_w}{R_p} - \frac{\mu}{2} \cdot F_0 \cdot p_b \tag{21}$$

$$\eta(t) = \frac{T_w(t) w_w}{T_p w_p} = \left[\frac{\left[T_p - \frac{\mu}{2} \cdot F_0 \cdot p_b \right] \cdot \frac{R_w}{R_p} - \frac{\mu}{2} \cdot F_0 \cdot p_b}{T_p} \right] \cdot \frac{1}{i} \tag{22}$$

- **Single tooth contact zone at right of pitch point, $t_a \le t < t_b$.**

Tooth contact point P1C lies along DC zone (see Figure 2):

$$T_w(t) = \left[T_p + \mu \cdot F_0 \cdot \overline{T_1 P_{1C}}(t) \right] \cdot \frac{R_w}{R_p} - \mu \cdot F_0 \cdot \overline{T_2 P_{1C}}(t) \tag{23}$$

$$\eta(t) = \frac{T_w(t) w_w}{T_p w_p} = \left[\frac{\left[T_p + \mu \cdot F_0 \cdot \overline{T_1 P_{1C}}(t) \right] \cdot \frac{R_w}{R_p} - \mu \cdot F_0 \cdot \overline{T_2 P_{1C}}(t)}{T_p} \right] \cdot \frac{1}{i} \tag{24}$$

- **Single tooth contact zone at left of pitch point, $t_b \le t < t_c$.**

Tooth contact point P1C lies along CB zone (see Figure 2):

$$T_w(t) = \left[T_p - \mu \cdot F_0 \cdot \overline{T_1 P_{1C}}(t) \right] \cdot \frac{R_w}{R_p} + \mu \cdot F_0 \cdot \overline{T_2 P_{1C}}(t) \tag{25}$$

$$\eta(t) = \frac{T_w(t) w_w}{T_p w_p} = \left[\frac{\left[T_p - \mu \cdot F_0 \cdot \overline{T_1 P_{1C}}(t) \right] \cdot \frac{R_w}{R_p} + \mu \cdot F_0 \cdot \overline{T_2 P_{1C}}(t)}{T_p} \right] \cdot \frac{1}{i} \tag{26}$$

where i is the gear ratio.

An equivalent procedure is usually used to calculate the loaded static transmission error (Amabili, 1997). With this set of equations three observations can be drawn. First, the time varying output torque $T_w(t)$ must be always lower than nominal output torque T_p*i. Second, gear power loss is higher in double contact zone due to presence of highest sliding velocities, and third, gear efficiency must be equal to 1 at pitch point, that is at this point wheel torque must be equal to input torque times gear ratio.

2.4 Alternative output torque for the dynamic model with internal action of friction force

Following the preceding reasoning, like as for internal action of friction force model, the output torque function for each contact zone may be written as

- **Double contact zone, $0 \le t < t_a$.**

First tooth contact point P1C lies along ED zone, and second tooth contact point P2C along BA zone (see Figure 2):

$$T_w(t) = \left[\frac{R_w - \frac{\mu}{2} \cdot p_b}{R_p + \frac{\mu}{2} \cdot p_b} \right] \cdot T_p \tag{27}$$

$$\eta(t) = \frac{T_w(t) w_w}{T_p w_p} = \left[\frac{R_w - \frac{\mu}{2} \cdot p_b}{R_p + \frac{\mu}{2} \cdot p_b} \right] \cdot \frac{1}{i} \tag{28}$$

- **Single contact zone at right of pitch point, $t_a \le t < t_b$.**

Tooth contact point P1C lies along DC zone (see Figure 2):

$$T_w(t) = \left[\frac{R_w - \mu \cdot \overline{T_2 P_{1C}}(t)}{R_p - \mu \cdot \overline{T_1 P_{1C}}(t)} \right] \cdot T_p \tag{29}$$

$$\eta(t) = \frac{T_w(t) w_w}{T_p w_p} = \left[\frac{R_w - \mu \cdot \overline{T_2 P_{1C}}(t)}{R_p - \mu \cdot \overline{T_1 P_{1C}}(t)} \right] \cdot \frac{1}{i} \tag{30}$$

- **Single contact zone at left of pitch point, $t_b \le t < t_c$.**

Tooth contact point P1C lies along CB zone (see Figure 2):

$$T_w(t) = \left[\frac{R_w + \mu \cdot \overline{T_2 P_{2C}}(t)}{R_p + \mu \cdot \overline{T_1 P_{1C}}(t)} \right] \cdot T_p \tag{31}$$

$$\eta(t) = \frac{T_w(t) w_w}{T_p w_p} = \left[\frac{R_w + \mu \cdot \overline{T_2 P_{2C}}(t)}{R_p + \mu \cdot \overline{T_1 P_{1C}}(t)} \right] \cdot \frac{1}{i} \tag{32}$$

3. NUMERICAL EXAMPLE OF A FZG TYPE C SPUR GEAR PAIR. RESULTS AND DISCUSSION.

In this section a numerical simulation of the developed models in the previous sections for a FZG type C gear pair is presented. Table 1 shows the main design parameters of a FZG type C gear pair (Winter, 1985). Specifically, this gear pair is mainly used in micropitting tests on the FZG test rig (Winter, 1985). Limited to a maximum speed of 3000 r/min, the FZG test rig allows a maximum torque of 534.5 Nm on the pinion.

The calculation of the contact stiffness was achieved using the KISSSOFT® software – calculation program for machine design (KISS soft AG). All dynamic simulations run under the assumptions of constant mesh damping ratio (ζ=0.05), lack of gear errors and no transversal movements (infinite transverse flexibility). All gear oscillations are considered exclusively along the meshing line.

Table 1. Geometry of the FZG type C gear pair (Winter, 1985)

Parameter [Units]	Pinion	Wheel
Number of teeth	16	24
Module [mm]	4.5	
Center distance [mm]	91.5	
Addendum diameter [mm]	82.45	118.35
Pressure angle [º]	20	
Addendum modification [/]	+0.182	+0.171
Face width [mm]	14	
Profile shift factor	0.1817	0.1715
Polar moment of inertia [kgm^2]	3.45e-4	15.24e-4

As referred before, all additional functions added to the base model were expanded into the Fourier series up to 150 harmonics to provide an adequate representation. Moreover, this procedure was also applied to generate the time varying mesh stiffness function as shown in Figure 3. The DTE of FZG type C gear is computed for all combinations of three different input variables: three pinion speeds (100, 1000 and 3000 rpm), two pinion torques (239.3 and 372.6 Nm), and two friction coefficients (0.04 and 0.08). The input torques correspond exactly to eighth and tenth stage of the FZG test rig.

The solutions of the differential equations of motion with 1 degree of freedom were obtained by numerical integration. Fourth and fifth order Runge-Kutta method (Howard, 2003) has been employed and executed in MATLAB® software.

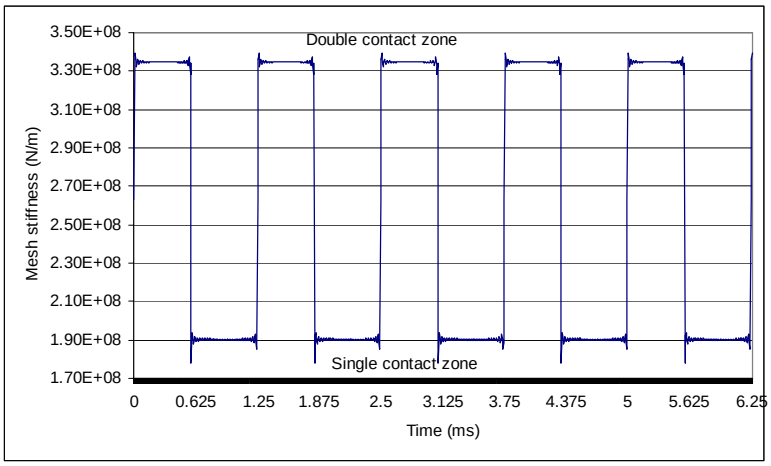

Figure 3. FZG type C gear mesh stiffness expressed by a Fourier series expansion with 150 harmonics.

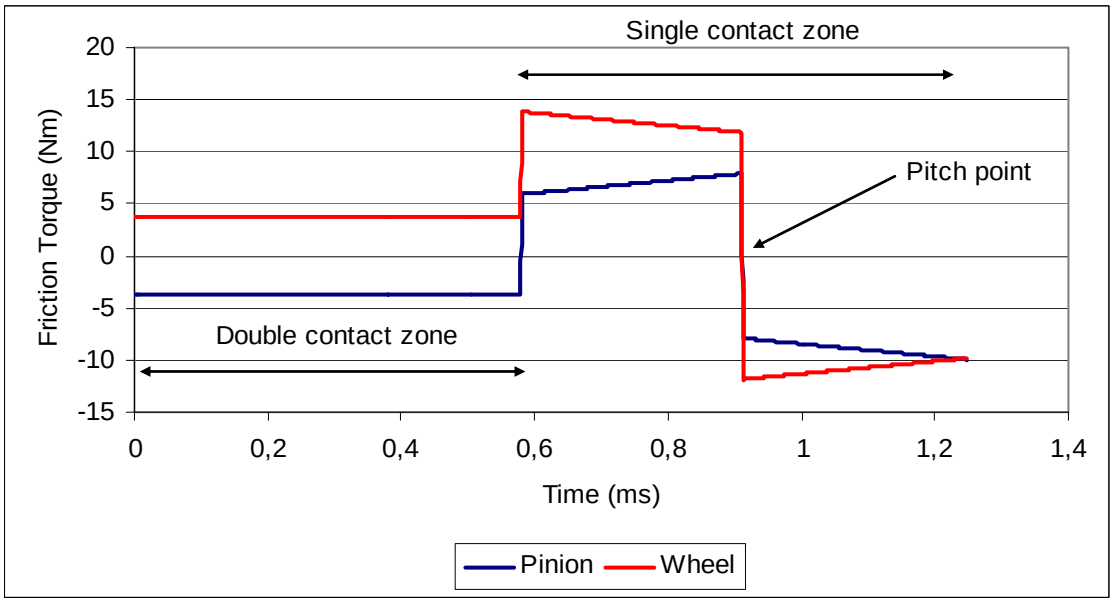

Figure 4. Example of pinion and wheel friction torques along line the meshing line.

In order to better understand the quantitative influence of tooth friction, we propose a representation of friction torques of pinion and wheel along meshing line. For simplicity consider the second model proposed above, where friction force is modelled as an external action. Based on the respective friction torque expressions $T_w(t)$ according the contact zone, Figure 4 shows pinion friction torque loss at double contact zone and single contact zone after the pitch point. Meanwhile, wheel friction torque loss takes place at double contact zone and single contact zone before the pitch point. It is interesting to verify that a simultaneous torque loss occurs at double contact zone, while at single contact zone a friction torque loss on the pinion corresponds to a torque gain on the wheel, and *vice versa*.

Figure 5 shows twelve DTE curves for the following presented models: base model, base model with friction force acting as an external excitation and base model with friction force acting as an internal excitation. All combinations of input torques, input speeds and constant mesh friction equal to 0.04 were simulated.

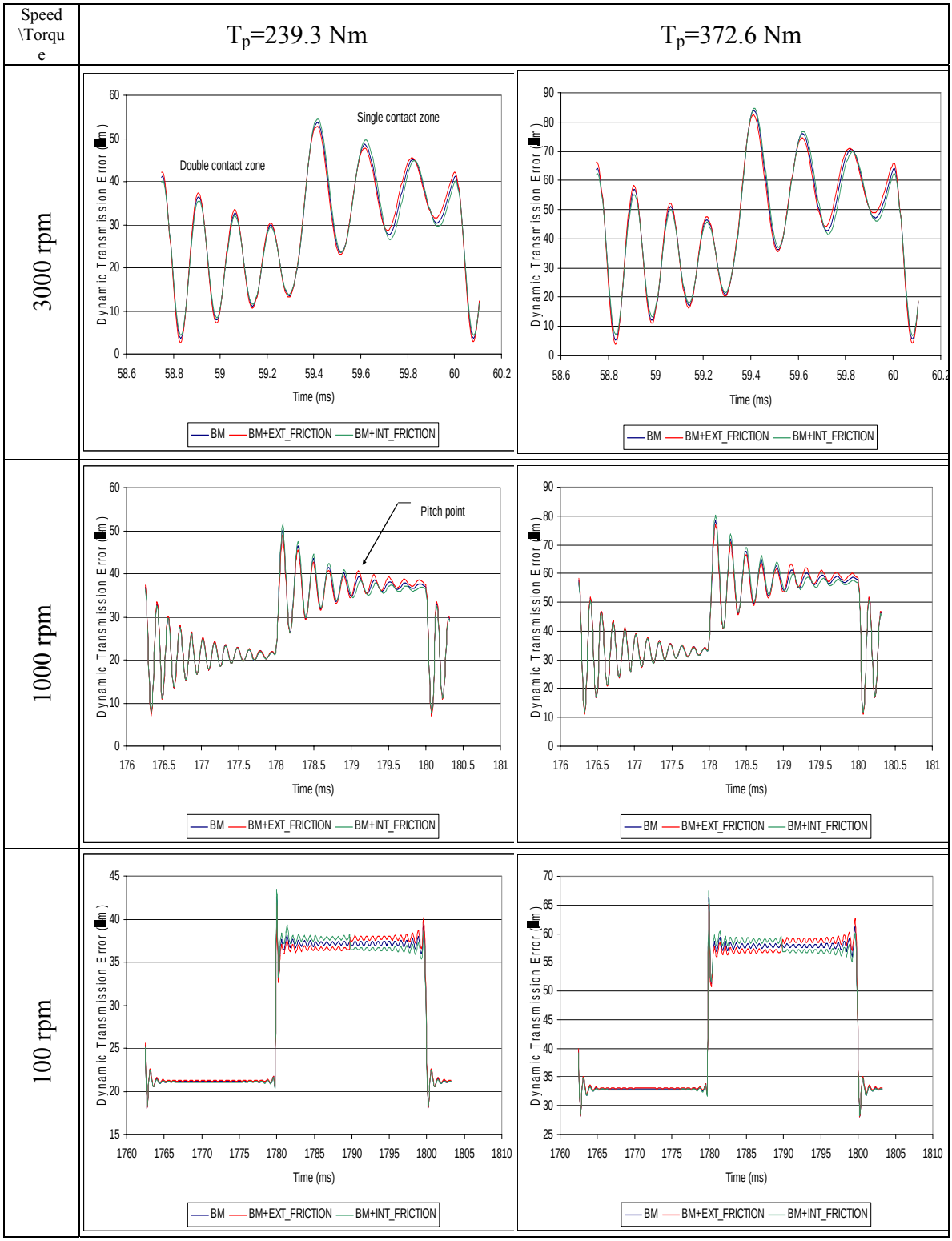

Figure 5. Dynamic transmission errors for 6 combinations of pinion velocity and torque with friction coefficient equal to 0.04.

On the basis of the dynamic responses, the following conclusions can be drawn:

- Higher input speeds correspond to higher DTE amplitudes and less number of oscillations at double and single contact zones;
- Higher input torques correspond to higher values of DTE;
- At 3000 rpm the three model's results seem indistincts, however pitch point transition is clearly evident for the other two input speeds;
- Taking the base model as reference and comparing results before and after the pitch point, a DTE's increase is verified for external model and a decrease for internal model.

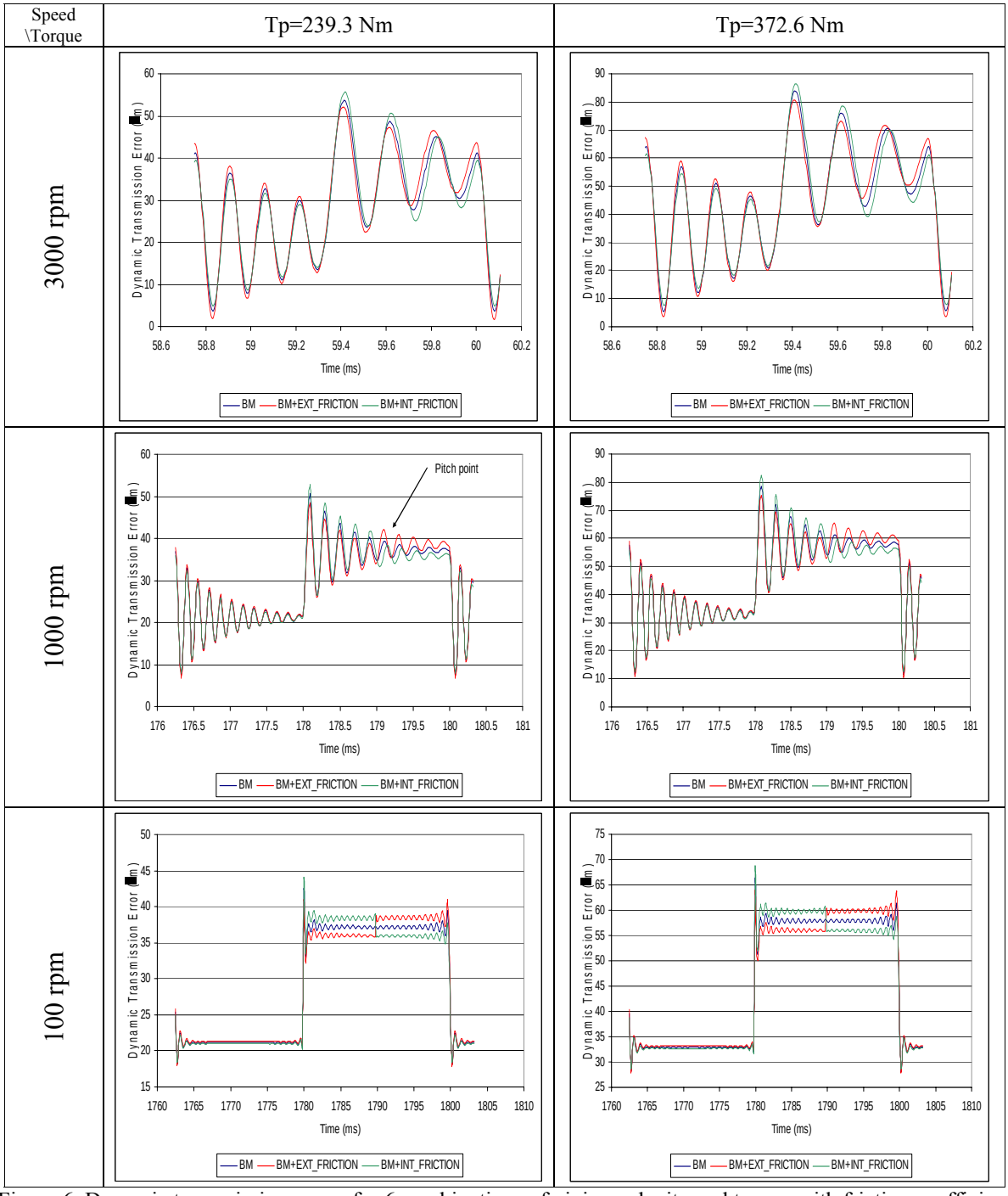

Figure 6. Dynamic transmission errors for 6 combinations of pinion velocity and torque with friction coefficient equal to 0.08.

The influence of friction can also be exhibited by doubling friction coefficient and maintaining other variables unchanged, as shown in Figure 6. At 3000 rpm noticeable differences between three models start to appear. For all speeds DTE oscillations around pitch point are now much more obvious, increasing and decreasing for external and internal model, respectively. By comparing frictionless model and two friction models with μ=0.04 and μ=0.08 the amplitude peaks are very similar.

Figure 7 shows the dynamic force between gear teeth along line of contact for two extreme operating conditions in terms of input torque and friction coefficient. Each graphic represents two double and one single (in the centre) contact zones. Having considered equal tooth load sharing, this implies that the dynamic force per tooth pair at single contact zone is two times larger than at double contact zone. The dynamic force oscillates around the static force along mesh cycle and once again it is clear the pitch point transition especially for the higher

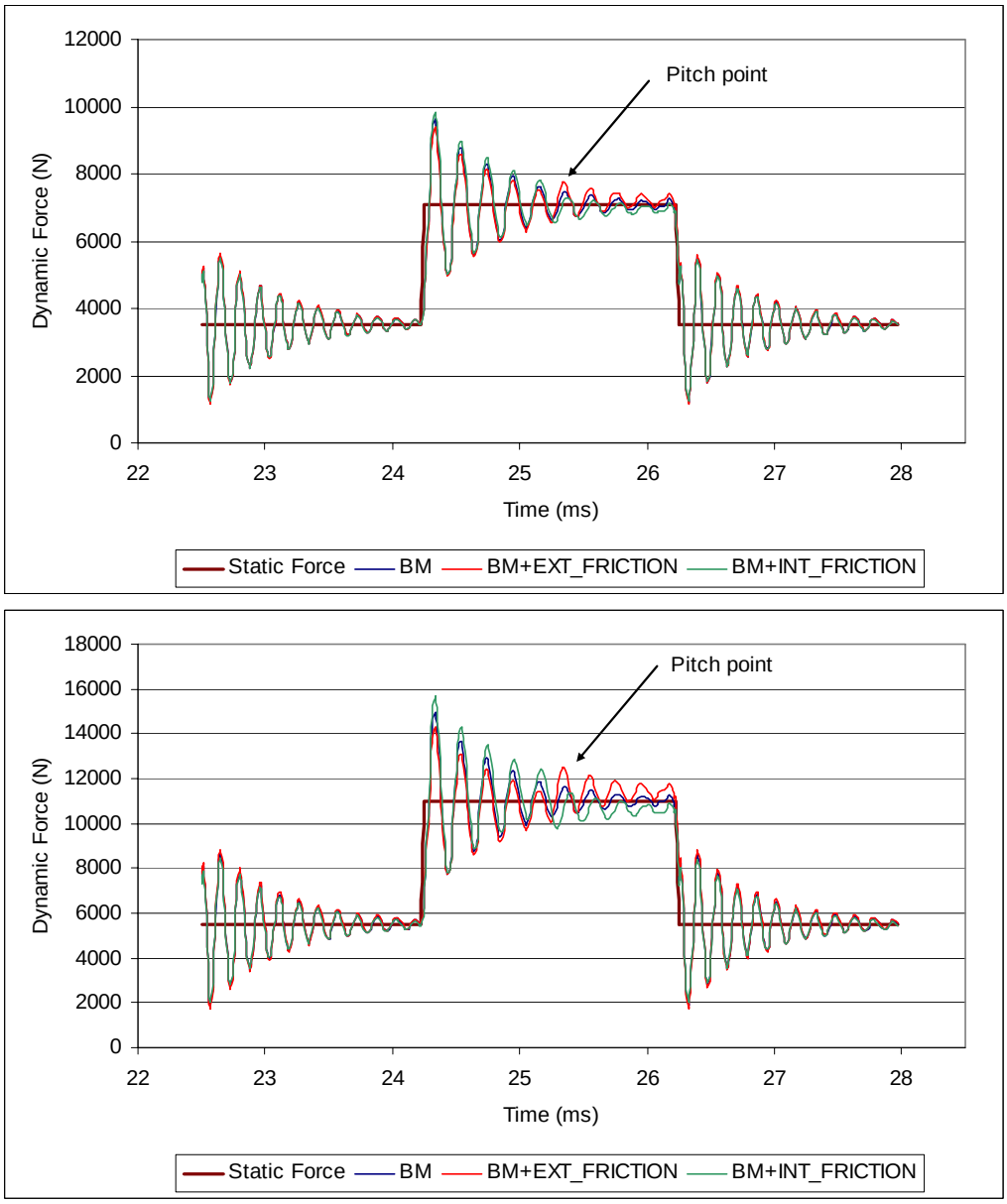

Figure 7. Dynamic forces in the gear contact for n_p=1000 rpm (T_p=239.3 Nm and μ=0.04 on left, and T_p=372.6 Nm and μ=0.08 on right).

friction coefficient. It is also interesting to compare dynamic and static forces along meshing line and conclude that former is in the range between 0.2 and 1.4 times the latter. This ratio is defined as dynamic factor, i.e. the ratio of maximum dynamic force to the maximum static force. Highest values are observed around double to single contact zone transition and lowest values from single to double transition. These results (pitch point steps) agree with those obtained by Vaishya, 2003 and Gunda, 2003, except for external excitation of friction where these authors detected a decrease of DTE around pitch point.

Other numerical results demonstrated that even if friction coefficient is duplicated, from 0.04 to 0.08, dynamic force peaks increase less than 2%, and an input speed decreasing causes a decreasing in the amplitude range of the dynamic force.

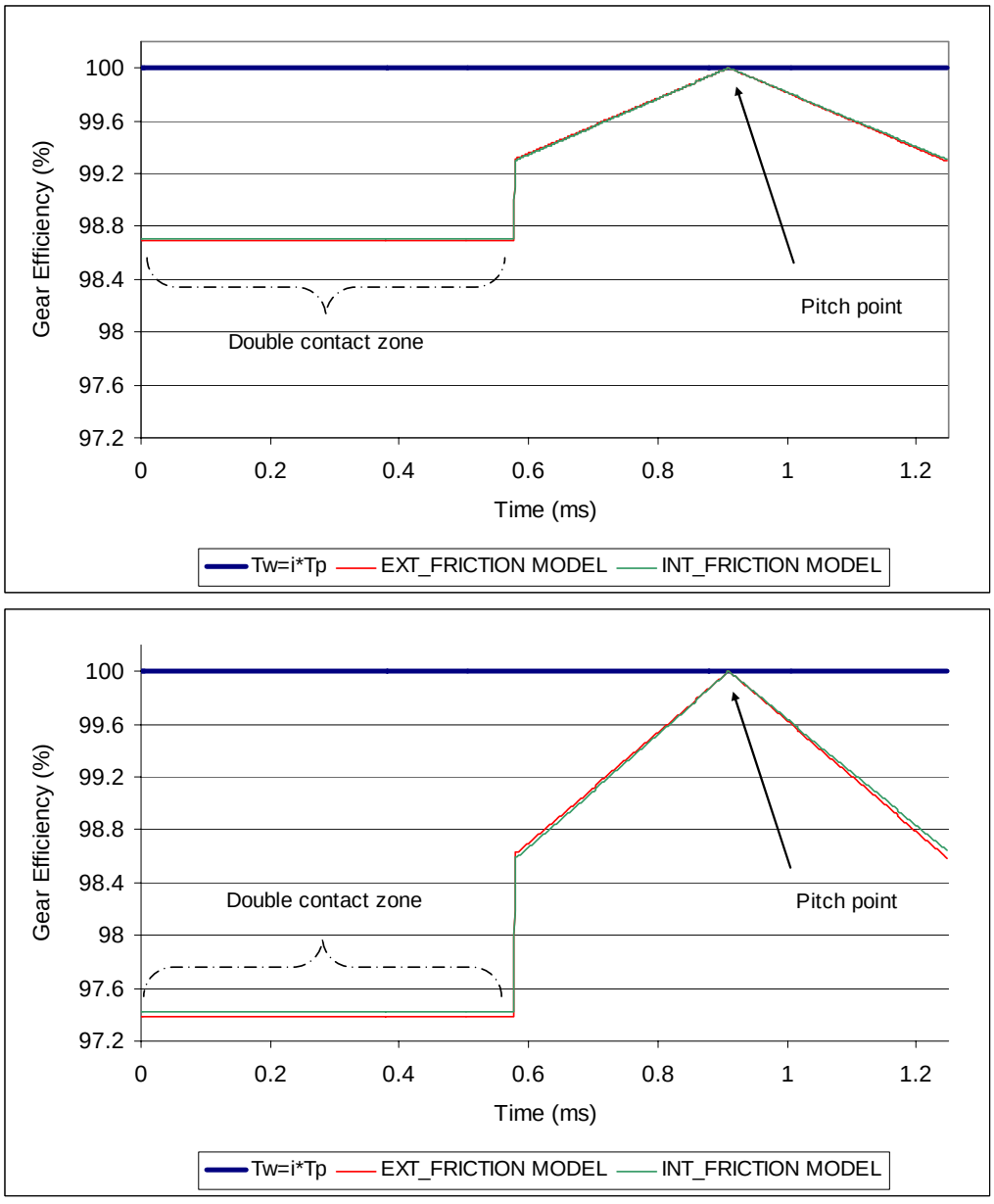

Figure 8. Gear efficiencies for external and internal formulations of friction excitation (T_p=239.3 Nm and μ=0.04 on left, and T_p=372.6 Nm and μ=0.08 on right).

Output torque alternatives of $T_w=i*T_p$ for both friction formulations have also been deducted and simulated. More specifically, dynamic characteristics of output torques result from constant friction parameter and periodically time-varying displacements of contact points along meshing line. In terms of gear efficiency three results may be expected. First, due to highest sliding velocity the gear efficiency at double contact zone is smaller than for single contact zone. Second, it must be 100% at pitch point because sliding velocity is zero, and third, higher friction coefficients may imply higher gear power losses, or lowest gear efficiencies. Figure 8 compares gear efficiencies of the three output torque formulations for two constant friction coefficients, 0.04 and 0.08. These functions are included in the dynamic models using Fourier series expansion with 150 harmonics. After confirming the three expected results, it is also important to note that the two curves of the output torque formulations are very close to each other, especially for the lower friction coefficient which has an average gear efficiency around 99.2%. For $\mu=0.08$ the average efficiency is equal to 98.4% and 98.43% for external and internal friction formulation, respectively. Furthermore, the efficiency of each friction coefficient along the meshing cycle is always inside the interval $97\% < \eta < 100\%$.

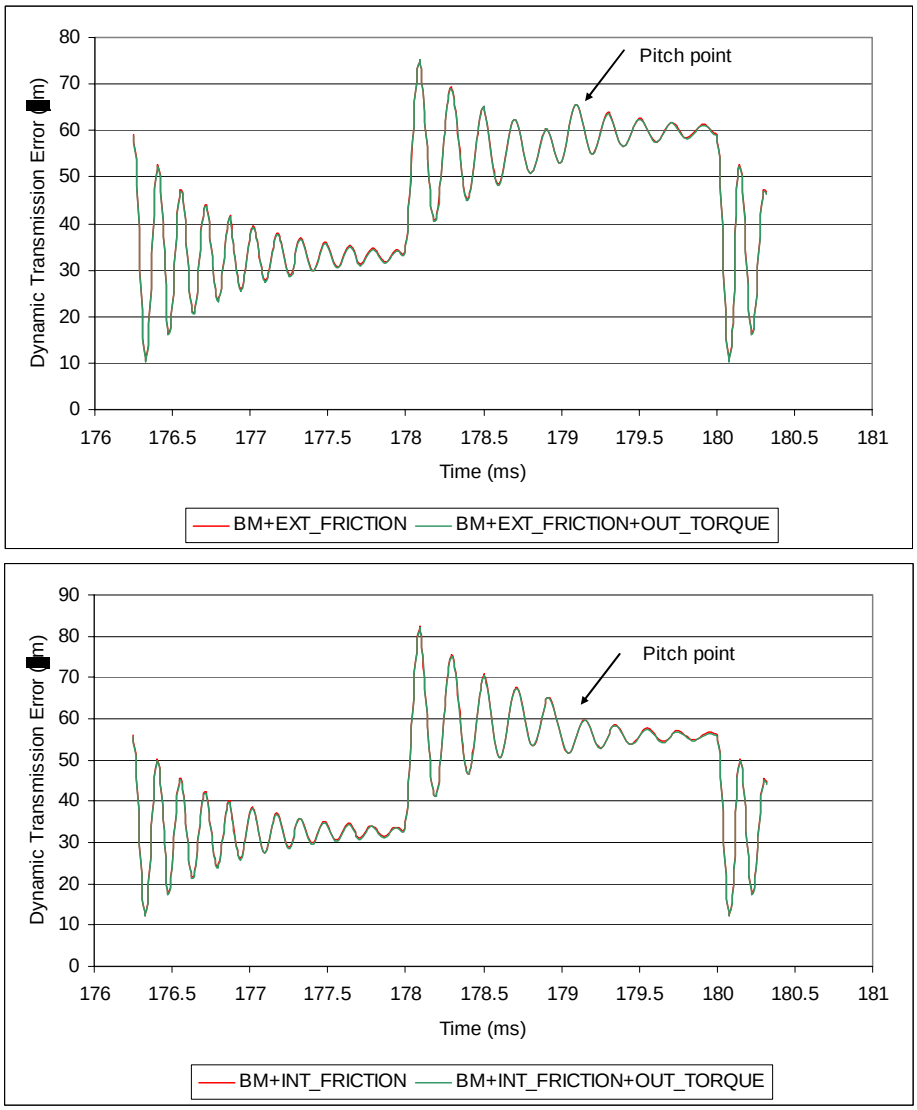

Figure 9. Influence of time varying output torques on FZG type C's friction dynamic models, T_p=372.6 Nm and μ=0.08.

Now let us consider the effect of the time-varying output torque on the FZG type C gear dynamics. The dynamic responses along gear meshing line for two friction formulations, external and internal action, with and without time varying output torques are presented in Figure 9.

From the comparison of graphics it is evident that incorporating time varying effects on output torques does not produce significative changes of dynamic responses. This is probably due to the fact of small output torque variations along meshing line $T_w/R_w \approx T_p/R_p$ when compared with theoretical one, given by $T_w=i*T_p$. This can explain why has been frequently assumed in literature that output torque presents small dynamic alteration (Kuang, 2001 and Gunda, 2003).

4. CONCLUSIONS

This article proposes a linear time varying dynamic model for studying the effect of friction force on FZG type C gear vibrations. A single degree of freedom torsional model including constant mesh damping and time varying mesh stiffness is first presented. Two extensions of this model considering external and internal friction force excitation and respective time varying output torque's alternatives are proposed. According to these formulations the following conclusions can be made:

1. Dynamic transmission error is significantly affected by the presence of friction force especially at pitch point, while before this point the two curves are very close to each other. If friction torque is modeled as an external excitation, the DTE's amplitudes at pitch point increase considerably (ex: 9% for μ=0.08, n_p=1000 and T_p=239.3Nm), but on the contrary decrease for an internal excitation (ex: -9.9% for μ=0.08, n_p=1000 and T_p=239.3Nm). Increasing the friction coefficient increases these pitch point steps. This phenomenon can also be easily observed in the dynamic forces between the meshing gear teeth, for example, an increase of +11.5% for external formulation and a decrease of -8.1% for internal formulation, booth with μ=0.08, n_p=1000 and T_p=239.3Nm.
2. Except for low input speeds the inter-teeth dynamic force along the meshing line oscillates between 0.2 and 1.4 times the static force, but the influence of friction on highest and lowest peaks of dynamic force is, however, weak.
3. The gear efficiencies were also considered into the dynamic model in order to quantify the impact of time varying output torques on gear dynamic transmission error amplitudes. It was shown that $T_w(t)$ has a little influence (ex: 1% for μ=0.08, n_p=1000 and T_p=372.6Nm) on both formulations of friction force (external and internal), probably due to small time output torque (or gear efficiency) variations along meshing line when compared with theoretical output.

A study of the effects of time varying friction coefficient along meshing line (or dynamic friction coefficients), unequal load sharing and gear errors is currently in progress.

REFERENCES

Amabili M. and Rivola A. Dynamic analysis of spur gear pairs: steady-state response and stability of the sdof model with time-varying meshing damping, Mechanical Systems and Signal Processing; Vol. 11(3); 1997; p. 375-390.

Gunda R. and Singh R. Dynamic analysis of sliding friction in a gear pair, Proceeding of DETC'03; Chicago; Illinois USA; September 2-6; 2003.

Howard I., Jia S. and Wang J. The dynamic modeling of a spur gear in mesh including friction and crack, Mechanical Systems and Signal Processing; Vol. 15(5); 2001; p. 831-853.

KISS soft AG: http://www.KISSsoft.ch/

Kuang J.H. and Lin A.D. The effect of tooth wear on the vibration spectrum of a spur gear pair, Journal of Vibration and Acoustics; Vol. 123; July 2001; p. 311-317.

Özguven H.N. and Houser D.R. Mathematical models used in gear dynamics – a review, Journal of Sound and Vibration; Vol. 121(3); 1988; p. 383-411.

Parey A. and Tandon N. Spur gear dynamic models including defects: a review, The Shock and Vibration Digest; Vol. 35; No. 6; November 2003; p. 465–478.

Vaishya M. and Singh R. Sliding friction-induced non-linearity and parametric effects in gear dynamics, Journal of Sound and Vibration; Vol. 248(4); 2001; p. 671-694.

Vaishya M. and Singh R. Strategies for modeling friction in gear dynamics, Journal of Mechanical Design; Vol. 125; June 2003; p. 383-393.

Velex P. and Sainsot P. An analytical study of tooth friction excitations in errorless spur and helical gears, Mechanism and Machine Theory; 37; 2002; p. 641-658.

Wilson H. B., Turcotte L. H. and Halpern D. Advanced mathematics and mechanics applications using MATLAB, Third Edition, CHAPMAN & HALL/CRC, 2003.

Winter, H. and Michaelis, K. FZG gear test rig – Description and possibilities. In: Coordinate European Council Second International Symposium on the performance evaluation of automotive fuels and lubricants, 1985.

APPENDIX A

In this appendix the analytical equations of absolute velocities of first P1C and second P2C points of contact, and respective sliding velocities along meshing line are presented. Figure 1A shows a Cartesian coordinate system Cntz with its origin at the reference point C (pitch point).

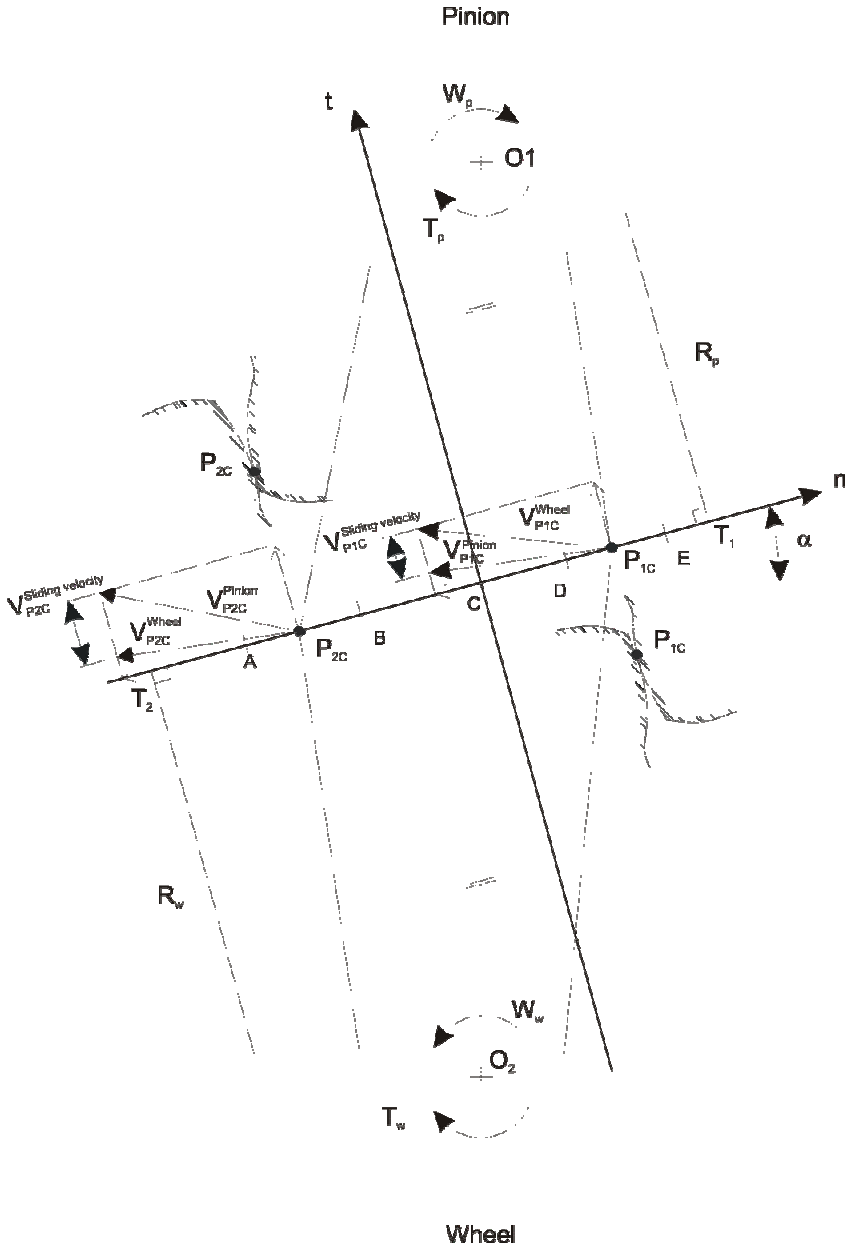

Figure 1A. Coordinate system for velocities of the first P1C and second P2C contact points.

Consider first the friction force definition between solids A and B,

$$\overrightarrow{F_a^{A/B}} = -\mu \cdot \left\| \overrightarrow{F_n} \right\| \cdot \frac{\overrightarrow{v_{A/B}}}{\left\| \overrightarrow{v_{A/B}} \right\|} \tag{A1}$$

The sliding velocity of first contact point P1C is

$$\begin{aligned}\overrightarrow{v_{gear/wheel\,P1C}} &= \overrightarrow{v_{O2P1C}} - \overrightarrow{v_{O1P1C}} = \\ &= \overrightarrow{v_{O2}} + \overrightarrow{w_{wheel}} \wedge \overrightarrow{O_2P1C} - \left[\overrightarrow{v_{O1}} + \overrightarrow{w_{pinion}} \wedge \overrightarrow{O_1P1C}\right] = \\ &= -\overrightarrow{v_{pinion/wheel\,P1C}}\end{aligned} \tag{A2}$$

with absolute velocities of first contact point P1C and respective position vectors defined as

$$\overrightarrow{v_{O1P1C}} = \overrightarrow{v_{O1}} + \overrightarrow{w_{pinion}} \wedge \overrightarrow{O_1P1C} \tag{A3}$$

$$\overrightarrow{v_{O2P1C}} = \overrightarrow{v_{O2}} + \overrightarrow{w_{wheel}} \wedge \overrightarrow{O_2P1C} \tag{A4}$$

$$\begin{aligned}\overrightarrow{O1P1C} &= \overrightarrow{O1T1} + \overrightarrow{T1P1C} = \\ &= \overrightarrow{O1T1} + \overrightarrow{T1E} + \overrightarrow{w_{pinion}} \wedge \overrightarrow{O_1T1} \cdot t\end{aligned} \tag{A5}$$

$$\begin{aligned}\overrightarrow{O2P1C} &= \overrightarrow{O2C} + \overrightarrow{CT1} + \overrightarrow{T1P1C} = \\ &= \overrightarrow{O2C} + \overrightarrow{CT1} + \overrightarrow{T1E} + \overrightarrow{w_{pinion}} \wedge \overrightarrow{O_1T1} \cdot t\end{aligned} \tag{A6}$$

The sliding velocity of second contact point P2C contact is

$$\begin{aligned}\overrightarrow{v_{wheel/pinion\,P2C}} &= \overrightarrow{v_{O2P2C}} - \overrightarrow{v_{O1P2C}} = \\ &= \overrightarrow{v_{O2}} + \overrightarrow{w_{gear}} \wedge \overrightarrow{O_2P2C} - \left[\overrightarrow{v_{O1}} + \overrightarrow{w_{pinion}} \wedge \overrightarrow{O_1P2C}\right] = \\ &= -\overrightarrow{v_{pinion/wheel\,P2C}}\end{aligned} \tag{A7}$$

with absolute velocities of second contact point P2C and respective position vectors defined as

$$\overrightarrow{v_{O1P2C}} = \overrightarrow{v_{O1}} + \overrightarrow{w_{pinion}} \wedge \overrightarrow{O_1P2C} \tag{A8}$$

$$\overrightarrow{v_{O2P2C}} = \overrightarrow{v_{O2}} + \overrightarrow{w_{wheel}} \wedge \overrightarrow{O_2P2C} \tag{A9}$$

$$\begin{aligned}\overrightarrow{O1P1C} &= \overrightarrow{O1T1} + \overrightarrow{T1P2C} = \\ &= \overrightarrow{O1T1} + \overrightarrow{T1E} + \overrightarrow{w_{pinion}} \wedge \overrightarrow{O_1T1} \cdot t\end{aligned} \tag{A10}$$

$$\begin{aligned}\overrightarrow{O2P2C} &= \overrightarrow{O2T1} + \overrightarrow{T1P2C} = \\ &= \overrightarrow{O2T1} + \overrightarrow{T1E} + \overrightarrow{EB} + \overrightarrow{w_{pinion}} \wedge \overrightarrow{O_1T1} \cdot t\end{aligned} \tag{A11}$$

Finally the friction forces of pinion and wheel at double contact zone for first P1C and second contact point P2C and assuming equal load share are expressed as

$$\overrightarrow{F_a P1C_{pinion}} = -\mu \cdot \frac{\left\|\overrightarrow{F_n}\right\|}{2} \cdot \frac{\overrightarrow{v_{pinion/wheel\,P1C}}}{\left\|\overrightarrow{v_{pinion/wheel\,P1C}}\right\|} \tag{A12}$$

$$\overrightarrow{F_a P2C_{pinion}} = -\mu \cdot \frac{\left\|\overrightarrow{F_n}\right\|}{2} \cdot \frac{\overrightarrow{v_{pinion/wheel\,P2C}}}{\left\|\overrightarrow{v_{pinion/wheel\,P2C}}\right\|} \tag{A13}$$

$$\overrightarrow{F_a P1C_{wheel}} = -\mu \cdot \frac{\left\|\overrightarrow{F_n}\right\|}{2} \cdot \frac{\overrightarrow{v_{wheel/pinion\,P1C}}}{\left\|\overrightarrow{v_{wheel/pinion\,P1C}}\right\|} \tag{A14}$$

$$\overrightarrow{F_a P2C_{wheel}} = -\mu \cdot \frac{\left\|\overrightarrow{F_n}\right\|}{2} \cdot \frac{\overrightarrow{v_{wheel/pinion\,P2C}}}{\left\|\overrightarrow{v_{wheel/pinion\,P2C}}\right\|} \tag{A15}$$

and for a single contact zone

$$\overrightarrow{F_a P1C_{pinion}} = -\mu \cdot \left\|\overrightarrow{F_n}\right\| \cdot \frac{\overrightarrow{v_{pinion/wheel\,P1C}}}{\left\|\overrightarrow{v_{pinion/wheel\,P1C}}\right\|} \tag{A16}$$

$$\overrightarrow{F_a P1C_{wheel}} = -\mu \cdot \left\|\overrightarrow{F_n}\right\| \cdot \frac{\overrightarrow{v_{wheel/pinion\,P1C}}}{\left\|\overrightarrow{v_{wheel/pinion\,P1C}}\right\|} \tag{A17}$$